

Photoneutron cross sections for neodymium isotopes: Toward a unified understanding of (γ, n) and (n, γ) reactions in the rare earth region

H.-T. Nyhus,¹ T. Renstrøm,¹ H. Utsunomiya,^{2,3} S. Goriely,⁴ D. M. Filipescu,⁵ I. Gheorghe,^{5,7} O. Tesileanu,⁵ T. Glodariu,⁶ T. Shima,⁸ K. Takahisa,⁸ S. Miyamoto,⁹ Y.-W. Lui,¹⁰ S. Hilaire,¹¹ S. Péru,¹¹ M. Martini,^{4,11,12} L. Siess,⁴ and A. J. Koning¹³

¹*Department of Physics, University of Oslo, N-0316 Oslo, Norway*

²*Department of Physics, Konan University, Okamoto 8-9-1, Kobe 659-8501, Japan*

³*Center for Nuclear Study, University of Tokyo, 2-1 Hirosawa, Wako, Saitama 351-0198, Japan*

⁴*Institut d'Astronomie et d'Astrophysique, Université Libre de Bruxelles, Campus de la Plaine, CP-226, 1050 Brussels, Belgium*

⁵*ELI-NP, "Horia Hulubei" National Institute for Physics and Nuclear Engineering (IFIN-HH), 30 Reactorului, 077125 Bucharest-Magurele, Romania*

⁶*"Horia Hulubei" National Institute for Physics and Nuclear Engineering (IFIN-HH), 30 Reactorului, 077125 Bucharest-Magurele, Romania*

⁷*Faculty of Physics, University of Bucharest, RO-077125, Bucharest, Romania*

⁸*Research Center for Nuclear Physics, Osaka University, Suita, Osaka 567-0047, Japan*

⁹*Laboratory of Advanced Science and Technology for Industry, University of Hyogo, 3-1-2 Kouto, Kamigori, Ako-gun, Hyogo 678-1205, Japan*

¹⁰*Cyclotron Institute, Texas A&M University, College Station, Texas 77843, USA*

¹¹*CEA, DAM, DIF, F-91297 Arpajon, France*

¹²*Department of Physics and Astronomy, Ghent University, Proeftuinstraat 86, B-9000 Gent, Belgium*

¹³*Nuclear Research and Consultancy Group, P.O. Box 25, NL-1755 ZG Petten, The Netherlands*

(Received 3 October 2014; revised manuscript received 20 November 2014; published 22 January 2015)

Photoneutron cross sections were measured for five stable Nd isotopes, ^{143,144,145,146,148}Nd, near neutron threshold with highly monochromatic laser-Compton scattering γ rays. The photoneutron data were compared with the calculations performed with the TALYS reaction code with inputs of the Skyrme Hartree-Fock-Bogoliubov (HFB) plus quasi-particle random phase approximation (QRPA) model and the axially symmetric deformed Gogny HFB plus QRPA model of $E1$ γ -ray strength. Using the γ -ray strength function constrained by the present photoneutron data, a thorough analysis of the reverse (n, γ) cross sections is made. Radiative neutron capture cross sections for an s-process branching-point nucleus in the rare earth region, ¹⁴⁷Nd with the half-life 10.98 d, are deduced with the γ -ray strength function method. The impact of the newly evaluated ¹⁴⁷Nd(n, γ)¹⁴⁸Nd cross section on s-process nucleosynthesis is discussed.

DOI: [10.1103/PhysRevC.91.015808](https://doi.org/10.1103/PhysRevC.91.015808)

PACS number(s): 25.20.Lj, 21.10.Pc, 25.40.Lw, 27.60.+j

I. INTRODUCTION

Radiative neutron capture on nuclei along the line of β stability in the medium- to heavy-mass region of the chart of nuclei is an important issue in nuclear astrophysics and nuclear engineering. In nuclear astrophysics, the cross sections are important to determine the s-process path at branching points where neutron capture and β decay compete [1]. The neutron capture data are also of essential importance for nuclear transmutation of long-lived fission products known as nuclear waste in the field of nuclear engineering [2]. Following the preceding paper for samarium isotopes [3], this paper for neodymium isotopes constitutes the second part of our investigations in the rare earth region.

Although experimental data of radiative neutron capture cross sections for stable nuclei are well documented [4], those for radioactive nuclei are scarce due to the difficulty of direct measurements that requires both an intense neutron beam and radioactive samples. While some of radioactive nuclei with half-lives ($T_{1/2}$) of the order of years have become objectives for direct measurements, for example, ¹⁵¹Sm ($T_{1/2} = 90$ yr) [5,6] and ⁶³Ni ($T_{1/2} = 100$ yr) [7] at CERN/n-TOF, ¹⁴⁷Pm ($T_{1/2} = 2.62$ yr) at Karlsruhe [8], ²⁴⁴Cm ($T_{1/2} = 18.1$ yr) [9] at J-Parc (Tokai), and ¹⁷³Lu ($T_{1/2} = 1.73$ yr) [10] in progress at LANSCE (Los Alamos), those with $T_{1/2}$ of the order of days and shorter are far beyond the experimental scope at present.

The well-established γ -ray strength function (γ SF) method can be used for constraining the (n, γ) cross sections for radioactive nuclei [11,12]. Relying on the Brink hypothesis [13] linking the photo-deexcitation process to photoabsorption, the method determines the γ SF which commonly quantifies radiative neutron capture and photoneutron cross sections. The (n, γ) cross section is governed by primary γ transitions from a neutron capture state at the excitation energy E to all possible nuclear states below the neutron threshold. Thus, the γ SF at γ -ray energies ε_γ below the neutron separation energy (S_n) and the nuclear level density at the final state ($E - \varepsilon_\gamma$) play an essential role in this capture reaction [14]. Photoneutron cross sections provide a stringent experimental constraint in absolute scale on the γ SF around S_n . When auxiliary (γ, γ') and particle- γ coincidence data that help to construct the γ SF below S_n are unavailable, the method requires a systematic measurement of photoneutron cross sections for neighboring stable isotopes of the radioactive nucleus of interest, in addition to existing (n, γ) data that serve as experimental constraints on the γ SF below S_n . Thus, a unified understanding of (n, γ) and (γ, n) cross sections throughout an isotopic chain offers detailed information on the γ SF for a given nucleus formed by neutron capture on the radioactive nucleus. Such a systematic approach with the γ SF method has been applied to zirconium [15], tin [16], and molybdenum [17] isotopes.

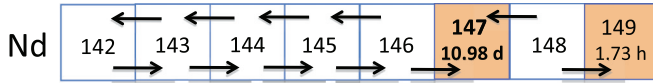


FIG. 1. (Color online) The chart of nuclei depicting our systematic analysis of (γ, n) and (n, γ) cross sections for Nd isotopes in the context of the γ -ray strength function method. Photonuclear cross sections measured in the present experiment are shown by left-pointing arrows. Radiative neutron capture cross sections discussed in the present systematic analysis are shown by right-pointing arrows. Photonuclear cross sections for the radioactive nucleus ^{147}Nd are deduced with the γ -ray strength function method.

Figure 1 depicts photonuclear emission (\leftarrow) and radiative neutron capture (\rightarrow) on Nd isotopes of interest in the present paper. We measured photonuclear cross sections for five neodymium isotopes, $^{143-146, 148}\text{Nd}$. Combining the present (γ, n) data with existing (n, γ) data for six Nd isotopes, $^{142-146, 148}\text{Nd}$, we determine $^{147}\text{Nd}(n, \gamma)$ cross sections with the γ SF method. The present systematic measurement included two odd- A nuclei, ^{143}Nd and ^{145}Nd , for which photonuclear cross sections are presented near the neutron threshold for the first time.

In this paper, we present radiative neutron capture cross sections for ^{147}Nd with $T_{1/2} = 10.98$ d, an s-process branching-point nucleus located in the rare earth region [1, 18]. Its β decay leads to the subsequent branchings at $^{147, 148}\text{Pm}$ [8], which in turn affect the s-process production ratio of ^{147}Sm to ^{148}Sm . We discuss a possible impact of the new cross section for ^{147}Nd on the abundance ratio of ^{148}Nd to the s-only nucleus ^{148}Sm in asymptotic giant branch (AGB) stars.

The outline of the paper is given as follows. A description of the experimental procedure and the data reduction is limited to a minimum in Sec. II, yielding a detailed description to the preceding paper [3]. The theoretical analysis of the photonuclear cross sections is given in Sec. III. The radiative neutron cross sections are analyzed in Sec. IV. The $^{147}\text{Nd}(n, \gamma)^{148}\text{Nd}$ cross section is determined with the γ SF method in Sec. V, followed by a possible impact of the cross section on the s-process nucleosynthesis in Sec. VI. Finally, conclusions are drawn in Sec. VII.

II. EXPERIMENT

The experiment was performed at the experimental hutch GACKO (Gamma Collaboration Hutch of Konan University) of the γ -ray beamline BL01 of the NewSUBARU synchrotron radiation facility [19]. In the BL01, energy-tunable and highly monochromatic γ -ray beams [20] are produced through inverse Compton scattering between Nd : YVO₄ laser photons ($\lambda = 1064$ nm) and relativistic electrons in the NewSUBARU storage ring. Fine pencil-like beams of the laser Compton scattering (LCS) γ rays were produced and measured with a $3.5'' \times 4.0''$ LaBr₃(Ce) detector. The response function of the LaBr₃(Ce) detector to the LCS γ rays was reproduced with a GEANT4 simulation code implemented with the kinematics of the laser inverse Compton scattering to obtain the energy distribution of the γ -ray beam. The energy spread of the LCS γ -ray beam with a low-energy tail was 1%–2% in full width at half

maximum (see Figs. 4 and 5 of [3]). Details of the GEANT4 simulation will be given in a forthcoming paper [21], where also a more in-depth description of the experimental setup can be found.

Samples of $^{143-146, 148}\text{Nd}$ enriched to 90.85%–98.07% all in the oxide form of Nd₂O₃ with areal densities of 1.35–2.78 g/cm² were encapsulated in pure-aluminum containers and irradiated with LCS γ -ray beams. The samples were dehydrated by baking at temperatures up to 393 °C for 4 h in vacuum before being placed inside the aluminum containers. The sample masses were determined by weighing the containers before and after the filling.

The γ -rays flux was determined by the pile-up method of Ref. [22] after detecting the beam with a $6'' \times 5''$ NaI(Tl) detector mounted at the end of the beamline. Typically 20% corrections were made for the transmission rate of the LCS γ rays through the NaI(Tl) detector.

Neutrons were detected with a high-efficiency 4π neutron detector consisting of 20 ^3He proportional counters embedded in a polyethylene moderator of $36 \times 36 \times 50$ cm³ fully covered by additional 5-cm-thick polyethylene plates with 1-mm-thick cadmium for background neutron suppression. Neutrons were moderated in the polyethylene before being detected with three rings of 4, 8, and 8 ^3He counters placed at distances of 3.8, 7.0, and 10.0 cm, respectively from the γ -ray beam axis. The average neutron energy was determined by the so-called ring-ratio technique originally developed by Berman and Fultz [23]. The total neutron detection efficiency is more than 60% for neutrons with energies less than 1 MeV. More details of the neutron detection can be found in Ref. [24]. Neutron detection efficiencies of the three rings were re-measured after the present experiment using a calibrated ^{252}Cf source with an emission rate of 2.27×10^4 s⁻¹ with 2.2% uncertainty at the National Metrology Institute of Japan. The measurement excellently reproduced the results obtained at the same institute in 2006.

Photonuclear cross sections are deduced with the Taylor expansion method [25], which takes into account the energy spread of the LCS γ -ray beam. Corrections were also made for the contributions to the cross section coming from the isotopic impurities in the Nd samples. The correction remains small, being 1%–7% for the energy spread of the highly monochromatic LCS γ -ray beam and 2% even for the isotopic impurities of the less-enriched (90.85% and 91.73%) $^{143, 145}\text{Nd}$ samples. The systematic uncertainty of the present cross sections is 4.4% with the breakdown of 3% in the photon flux and 3.2% in the neutron detection efficiency.

Our photonuclear cross sections are compared in Fig. 2 with the Saclay measurements [26]. While a good agreement is obtained in the $^{146, 148}\text{Nd}$ cases, significant discrepancies are observed for the light Nd isotopes. In particular, our experiment leads to cross sections lower by typically 30% for ^{143}Nd , 20% for ^{144}Nd , and 27% for ^{145}Nd . Such an overestimate by the Saclay photodata was also reported in previous comparisons for ^{142}Nd with a renormalization by 0.86 [27], for ^{144}Sm by 0.80 [28], and for $^{\text{nat}}\text{Rb}$, $^{\text{nat}}\text{Sr}$, ^{89}Y , ^{90}Zr , ^{93}Nb , ^{127}I , ^{197}Au , and ^{208}Pb by a factor of 0.80–0.93 [29].

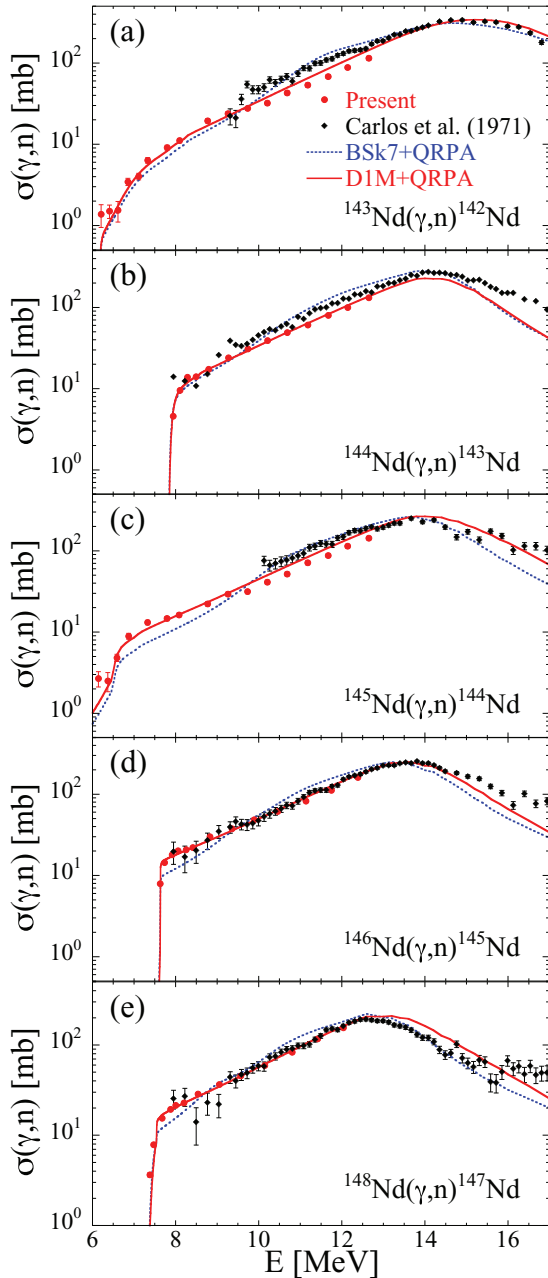


FIG. 2. (Color online) Comparison between the present photoneutron emission cross sections and previously measured ones [26] for $^{143-146,148}\text{Nd}$. Also included are the predictions from Skyrme HFB + QRPA (based on the BSk7 interaction) [32] and axially deformed Gogny HFB + QRPA models (based on the DIM interaction) [34].

III. THEORETICAL ANALYSIS

A. Photoneutron cross sections

Our new photoneutron cross sections shown in Fig. 2 have been compared to theoretical calculations obtained with the TALYS nuclear reaction code [30,31] and two different models of the γ SF, namely, the Skyrme Hartree-Fock-Bogoliubov (HFB) plus quasi-particle random phase approximation (QRPA) model [32] based on the BSk7 interaction

and the axially symmetric deformed Gogny HFB plus QRPA model [33–35] based on the DIM interaction [36]. The BSk7+QRPA model introduces phenomenological corrections to take the damping of the collective motion as well as the deformation effects into account. (Note, however, that deformation parameters are consistently extracted from the HFB-7 mass model based on the BSk7 Skyrme functional [37].) In contrast, the DIM + QRPA model allows for a consistent description of axially symmetric deformations and includes phenomenologically the impact of multiparticle-multihole configurations as a function of their densities [34]. Both models have proven their capacity to reproduce experimental photoabsorption data relatively well.

As seen in Fig. 2, cross sections around the neutron threshold are rather well described by the DIM + QRPA model, although some deviations can be seen. The agreement around the neutron threshold is rather satisfactory and there is no reason to invoke the presence of extra low-lying strength from the present data, at least in the vicinity of the neutron threshold, as seen in some previous photodata [11,15,16,38]. In contrast, larger deviations are seen for the predictions obtained with the BSk7 + QRPA strength, in particular around 11 MeV, but also at lower energies in the $^{145,146}\text{Nd}$ cases.

B. Radiative neutron capture cross sections

We now turn to the reverse radiative neutron capture channel. It should be kept in mind that the corresponding cross section for incident keV neutrons depends sensitively on the γ SF, but in a rather lower energy range below the neutron threshold, typically around 6 MeV of γ -ray energy. The predicted tail of the γ SF at low energies therefore plays a fundamental role.

On the basis of the Gogny HFB plus QRPA γ -ray strength [34], the reverse radiative neutron capture cross sections are now estimated with the TALYS reaction code [30,31] for the stable and experimentally known $^{142-146,148}\text{Nd}$ isotopes and compared with experimental cross sections in Fig. 3. In addition to the $E1$ strength function, the cross section calculation also depends on the adopted nuclear level density. We have used here the temperature-dependent HFB plus combinatorial model [39] normalized to the experimental s -wave spacing D_0 values at the neutron binding energy [14]. Note that experimental s -wave spacings are available, so uncertainties related to the adopted NLD model are rather small, typically 10%, as shown in Fig. 3, where the hashed areas correspond to uncertainties on experimental D_0 values. Similarly, the uncertainties related to the adopted neutron optical potential are negligible in the energy range of astrophysical interest, i.e., in the keV–MeV region.

Based on the radiative neutron capture cross section, the laboratory (i.e., without including the contribution of excited states) Maxwellian-averaged cross sections (MACS) have been estimated and compared with experimental data at an energy of $kT = 30$ keV in Table I. The theoretical error bars stem from the NLD uncertainties affecting the D_0 values. Here also, our TALYS predictions are compatible with experimental data, with theoretical values being usually higher than the measurements, except in the ^{142}Nd and ^{144}Nd cases.

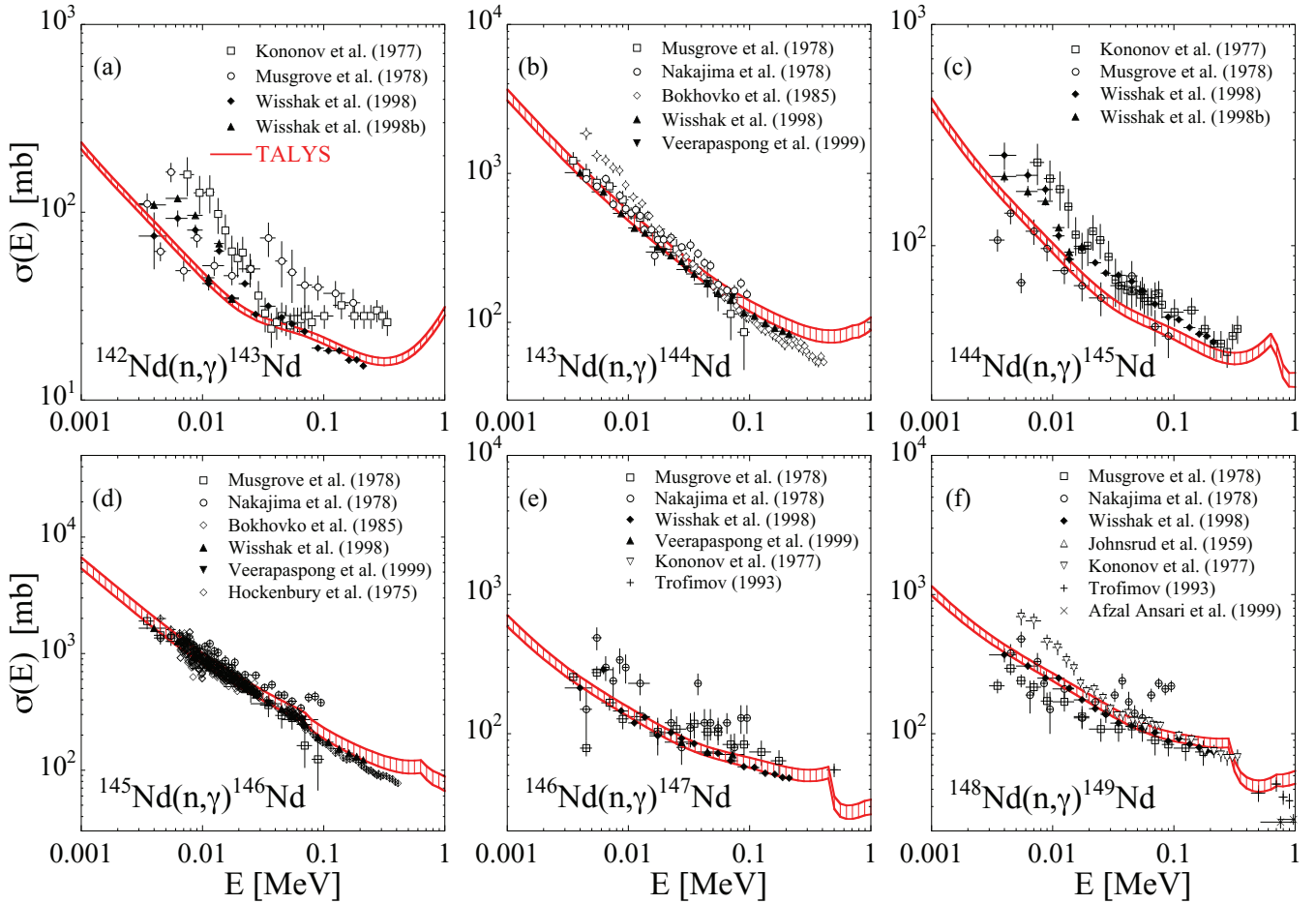


FIG. 3. (Color online) Comparison between the measured radiative neutron capture cross sections [40–50] with TALYS calculations making use of the DIM + QRPA $E1$ strength (solid line). The hashed area corresponds to uncertainties related to the NLD model and their normalization on experimental s -wave spacings at the neutron binding energy.

It should however be stressed that the MACS [42,43] have been measured relative to the radiative neutron capture cross section of ^{197}Au , which has been recently re-evaluated and found to deviate systematically by more than 5% from the cross section that is recommended as a reference for astrophysical applications [51].

As a conclusion, the TALYS calculation agrees well with the most recent experimental data for all six stable Nd isotopes, which shows that, within the uncertainties affecting the experimental γ SF and D_0 value, all γ SF data are compatible

TABLE I. Comparison of experimental (laboratory) MACS of stable Nd isotopes [42,43] with the TALYS predictions at an energy of 30 keV. MACS are given in millibarns.

Target	Exp. [42,43]	TALYS
^{142}Nd	35.0 ± 0.7	31 ± 2
^{143}Nd	245 ± 3	267 ± 23
^{144}Nd	81.3 ± 1.5	63 ± 4
^{145}Nd	425 ± 5	478 ± 50
^{146}Nd	91.2 ± 1	96 ± 8
^{148}Nd	147 ± 2	157 ± 11

with both the photoabsorption above the threshold and the radiative capture channels below the threshold.

C. Determination of the $^{147}\text{Nd}(n,\gamma)^{148}\text{Nd}$ cross section

The γ SF method can now be applied to the experimentally unknown cross section $^{147}\text{Nd}(n,\gamma)^{148}\text{Nd}$ by making use of the same nuclear inputs. In the case of ^{148}Nd , experimental information exists on the resonance spacing at the neutron binding energy, namely, $D_0 = 4.0 \pm 1.5$ eV [14]. The 40% error on D_0 corresponds to the major uncertainty still affecting the prediction of the $^{147}\text{Nd}(n,\gamma)^{148}\text{Nd}$ cross section, giving rise to a range of predicted cross sections within typically 20%–30%, as shown in Fig. 4. The ENDF/B-VII.1 evaluation [52] is seen to be in relatively good agreement with our estimate, but the ROSFOND-2010 evaluation [53] gives rather lower cross sections above typically a few keV and the JENDL-4.0 evaluation [54] gives larger values above typically 100 keV. The resulting MACS of astrophysical interest are shown in Fig. 5 and compared with the theoretical determination recommended in Ref. [55]. Our MACS (and, consequently, also the ENDF/B-VII.1 and JENDL-4.0 ones) are found to be significantly larger than those of the previous recommendation [55]. In particular, at 30 keV, our cross section

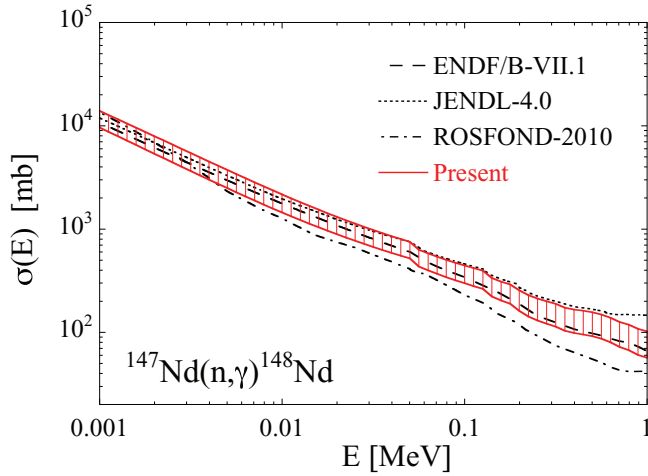


FIG. 4. (Color online) Prediction of the $^{147}\text{Nd}(n,\gamma)^{148}\text{Nd}$ cross section. The dotted, dashed, and dash-dotted curves correspond to the JENDL-4.0 [54], ENDF/B-VII.1 [52], and ROSFOND-2010 [53] evaluations.

amounts to 880 ± 170 mb, to be compared with 544 ± 90 mb recommended in Ref. [55] and theoretical values ranging between 387 and 663 mb from various statistical model calculations and compiled in the KADONIS library [56].

IV. APPLICATION TO s-PROCESS NUCLEOSYNTHESIS IN AGB STARS

Even though the observation of radioactive Tc in stellar envelopes [57] clearly proves that the s-process takes place during the hydrostatic burning phases of a star, it remains difficult to explain the origin of the large neutron concentrations required to produce s elements. Two nuclear reactions are suggested as possible neutron sources, i.e., $^{13}\text{C}(\alpha,n)^{16}\text{O}$ and $^{22}\text{Ne}(\alpha,n)^{25}\text{Mg}$. These reactions could be responsible for a large production of neutrons during the

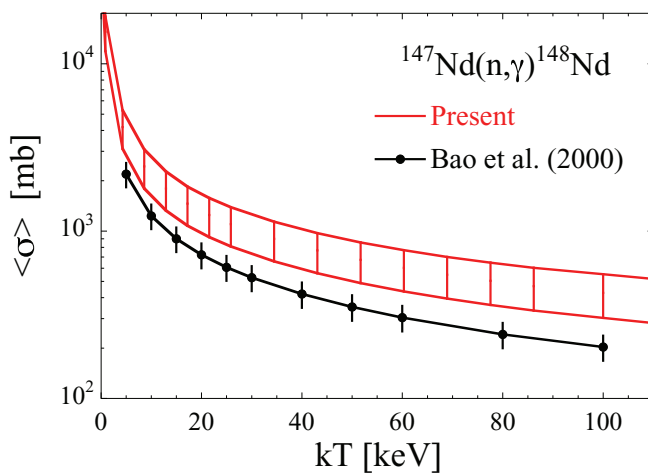


FIG. 5. (Color online) Comparison between our newly determined $^{147}\text{Nd}(n,\gamma)^{148}\text{Nd}$ MACS with the values recommended in Ref. [55].

given burning phases, namely, the core He-burning of massive stars (heavier than $10M_{\odot}$) and the shell He-burning during the thermal AGB instabilities (thermal pulses) of low- and intermediate-mass stars ($<10M_{\odot}$) [1,58]. The core He-burning of solar-metallicity stars has proved its ability to produce the lightest s elements (i.e., $70 \lesssim A \lesssim 90$), but since ^{22}Ne is a secondary source, the efficiency remains identical for metal-poor stars. The astrophysical models underlying the thermal pulse scenario (believed to be responsible for the production of the $A > 90$ s elements) remain quite uncertain in many respects, in particular in the description of the mixing mechanisms that could be at the origin of the neutron production. AGB models including diffusive overshoot or rotational effects suggest the partial mixing of protons (PMP) from the H-rich envelope into the C-rich layers during the third dredge-up [59–61]. In low-mass AGB stars of typically 1 to $3M_{\odot}$, this PMP model has been successful in explaining the main and strong components of the s-process, including the production of Nd and Sm isotopes. In more massive AGB stars, such an s-process during the interpulse might be inhibited due to the high temperatures encountered at the base of the convective envelope and the resulting combustion of protons during the partial mixing [62]; the large temperatures can however lead to a significant neutron irradiation within the convective thermal pulse due to the activation of the $^{22}\text{Ne}(\alpha,n)^{25}\text{Mg}$ reaction [63].

Based on measured Maxwellian-averaged neutron capture cross sections of the stable Nd nuclei, the production of Nd and Sm isotopes by the s-process has already been studied in detail [8,42,43,64]. Our new estimation of the $^{147}\text{Nd}(n,\gamma)^{148}\text{Nd}$ cross section may however affect the s-process production of the sr nucleus ^{148}Nd and the s-only ^{148}Sm . To illustrate the impact of the newly determined MACS,

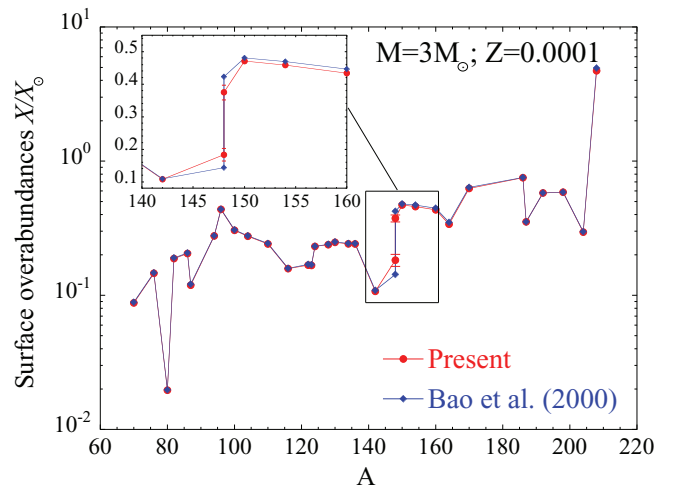


FIG. 6. (Color online) Final surface abundances X for a $3M_{\odot}$ AGB model star of metallicity $Z = 0.0001$ with respect to the solar values X_{\odot} for all s-only nuclei and ^{148}Nd as a function of the mass number A . The circles (including error bars) are obtained with the present $^{147}\text{Nd}(n,\gamma)^{148}\text{Nd}$ MACS and the diamonds with the values given in Ref. [55]. The insert shows an enlargement of the $140 \leq A \leq 160$ region.

nucleosynthesis calculations have been performed within the PMP model [61] in $3M_{\odot}$ AGB model stars for three different metallicities, namely, $Z = Z_{\odot} = 0.0123$, $Z = 0.004$, and $Z = 0.0001$ [65]. Our upper value for the $^{147}\text{Nd}(n,\gamma)^{148}\text{Nd}$ cross section, which is about twice as large as the one quoted in the widely used compilation of Ref. [55], leads to a larger production of ^{148}Nd by 40% and a corresponding reduction in ^{148}Sm production by about 10%. The final surface overabundances for the low-metallicity $Z = 0.0001$ star are illustrated in Fig. 6. In this specific case, if we use the upper limit of the cross section, we end up with an abundance ratio $[\text{}^{148}\text{Nd}/\text{}^{148}\text{Sm}] = \log[X(\text{}^{148}\text{Nd})/X_{\odot}(\text{}^{148}\text{Nd})] - \log[X(\text{}^{148}\text{Sm})/X_{\odot}(\text{}^{148}\text{Sm})] = -0.24$ (where X is the mass fraction), while the previously used rate [55] gives -0.47 . In other words, in low-metallicity stars, ^{148}Nd can be relatively produced with respect to the s-only nucleus ^{148}Sm , but also production could be significantly greater with our new upper limit, as seen in Fig. 6. In the case of the $Z = 0.004$ and $Z = Z_{\odot}$ model stars, we find a significantly lower production of ^{148}Nd with respect to ^{148}Sm , namely, $[\text{}^{148}\text{Nd}/\text{}^{148}\text{Sm}] = -0.46$ and -0.64 , respectively, with our rate and -0.68 and -0.82 , respectively, with the low rate of Ref. [55].

V. CONCLUSIONS

The γ SF method has been applied to the Nd isotopic chain in order to determine the radiative neutron capture cross section of the unstable ^{147}Nd isotope of astrophysical

interest. Based on an extensive analysis of five newly measured photoneutron cross sections and the inverse radiative neutron capture cross sections, the nuclear reaction ingredients have been constrained, leading to a final $^{147}\text{Nd}(n,\gamma)^{148}\text{Nd}$ cross section about 60% larger than the unconstrained value adopted in nucleosynthesis calculations. Our new rate determination leads to an increase of ^{148}Nd production and a decrease of the s-only ^{148}Sm abundance by the s-process in AGB stars.

ACKNOWLEDGMENTS

This work was supported by the Japan Private School Promotion Foundation and partly by the JSPS-FNRS bilateral program. We are grateful to M. Igashira of the Tokyo Institute of Technology for making the $^{143,145,146}\text{Nd}$ samples available to the present experiment. We thank Florin Rotaru of the National Institute for Physics and Nuclear Engineering Horia Hulubei for initiating us into GEANT4 coding and for fruitful discussions. We acknowledge PRACE for awarding us access to the resource CURIE based in France at TGCC-CEA. D. M. Filipescu, O. Tesileanu and I. Gheorghe acknowledge financial support from the Extreme Light Infrastructure Nuclear Physics (ELI-NP) Phase I, a project co-financed by the Romanian Government and the European Union through the European Regional Development Fund (425/12.12.2012, POS CCE, ID 1334 SMIS-CSNR 40741). H.-T. Nyhus and T. Renstrøm acknowledge financial support from the Norwegian Research Council (NFR), Project No. 210007. S. Goriely acknowledges financial support from the F.N.R.S.

-
- [1] F. Käppeler, R. Gallino, S. Bisterzo, and W. Aoki, *Rev. Mod. Phys.* **83**, 157 (2011).
- [2] IAEA-TECDOC-985, IAEA report, November 1997.
- [3] D. M. Filipescu *et al.*, *Phys. Rev. C* **90**, 064616 (2015).
- [4] <https://www-nds.iaea.org/exfor/exfor.htm>
- [5] K. Wisshak, F. Voss, F. Käppeler, M. Krtička, S. Raman, A. Mengoni, and R. Gallino, *Phys. Rev. C* **73**, 015802 (2006).
- [6] S. Marrone *et al.*, *Phys. Rev. C* **73**, 034604 (2006).
- [7] C. Lederer *et al.*, *Phys. Rev. C* **89**, 025810 (2014).
- [8] R. Reifarth *et al.*, *Astrophys. J.* **582**, 1251 (2003).
- [9] A. Kimura *et al.*, *J. Nucl. Sci. Technol.* **49**, 708 (2012).
- [10] https://www.oecd-nea.org/science/wpec/meeting2014/Exp_USA.pdf
- [11] H. Utsunomiya *et al.*, *Phys. Rev. C* **80**, 055806 (2009).
- [12] H. Utsunomiya *et al.*, *Phys. Rev. C* **82**, 064610 (2010).
- [13] D. M. Brink, Ph.D thesis, Oxford University, 1955.
- [14] R. Capote *et al.*, *Nucl. Data Sheets* **110**, 3107 (2009).
- [15] H. Utsunomiya *et al.*, *Phys. Rev. C* **81**, 035801 (2010).
- [16] H. Utsunomiya *et al.*, *Phys. Rev. C* **84**, 055805 (2011).
- [17] H. Utsunomiya *et al.*, *Phys. Rev. C* **88**, 015805 (2013).
- [18] M. Wiescher, F. Käppeler, and K. Langanke, *Annu. Rev. Astron. Astrophys.* **50**, 165 (2012).
- [19] S. Amano *et al.*, *Nucl. Instrum. Methods Phys. Res. A* **602**, 337 (2009).
- [20] K. Horikawa, S. Miyamoto, S. Amano, and T. Mochizuki, *Nucl. Instrum. Methods Phys. Res. A* **618**, 209 (2010).
- [21] I. Gheorghe *et al.* (unpublished).
- [22] T. Kondo *et al.*, *Nucl. Instrum. Methods A* **659**, 462 (2011).
- [23] B. L. Berman and S. C. Fultz, *Rev. Mod. Phys.* **47**, 713 (1975).
- [24] O. Itoh *et al.*, *J. Nucl. Sci. Technol.* **48**, 834 (2011).
- [25] H. Utsunomiya *et al.*, *Phys. Rev. C* **74**, 025806 (2006).
- [26] P. Carlos, H. Beil, R. Bergere, A. Lepretre, and A. Veysiere, *Nucl. Phys. A* **172**, 437 (1971).
- [27] C. T. Angell *et al.*, *Phys. Rev. C* **86**, 051302(R) (2012).
- [28] C. Nair *et al.*, *Phys. Rev. C* **81**, 055806 (2010).
- [29] B. L. Berman, R. E. Pywell, S. S. Dietrich, M. N. Thompson, K. G. McNeill, and J. W. Jury, *Phys. Rev. C* **36**, 1286 (1987).
- [30] A. J. Koning, S. Hilaire, and M. Duijvestijn, in *Nuclear Data for Science and Technology*, edited by O. Bersillon, F. Gunsing, E. Bauge, R. Jacqmin, and S. Leray (EDP Sciences, Les Ulis, France, 2008), p. 211.
- [31] A. J. Koning and D. Rochman, *Nucl. Data Sheets* **113**, 2841 (2012).
- [32] S. Goriely, E. Khan, and M. Samyn, *Nucl. Phys. A* **739**, 331 (2004).
- [33] S. Péru and H. Goutte, *Phys. Rev. C* **77**, 044313 (2008).
- [34] M. Martini, S. Hilaire, S. Goriely, A. J. Koning, and S. Péru, *Nucl. Data Sheets* **118**, 273 (2014).
- [35] S. Péru and M. Martini, *Eur. Phys. J. A* **50**, 88 (2014).
- [36] S. Goriely, S. Hilaire, M. Girod, and S. Péru, *Phys. Rev. Lett.* **102**, 242501 (2009).
- [37] S. Goriely, M. Samyn, M. Bender, and J. M. Pearson, *Phys. Rev. C* **68**, 054325 (2003).
- [38] T. Kondo *et al.*, *Phys. Rev. C* **86**, 014316 (2012).

- [39] S. Hilaire, M. Girod, S. Goriely, and A. J. Koning, *Phys. Rev. C* **86**, 064317 (2012).
- [40] V. N. Kononov, B. D. Jurlov, E. D. Poletaev, V. M. Timokhov, and G. N. Manturov, *Yad. Konstany* **22**, 29 (1977).
- [41] A. R. DeL. Musgrove, B. J. Allen, J. W. Boldeman, and R. L. Macklin, *Proceedings of the International Conference on Neutron Physics and Nuclear Data for Reactors and Other Applied Purposes* (Harwell, United Kingdom, 1978), p. 449.
- [42] K. Wisshak, F. Voss, F. Käppeler, L. Kazakov, and G. Reffo, *Phys. Rev. C* **57**, 391 (1998).
- [43] K. Wisshak, F. Voss, and F. Käppeler, *Phys. Rev. C* **57**, 3452 (1998).
- [44] Y. Nakajima, A. Asami, Y. Kawarasaki, and Y. Furuta, *Proc. International Conference on Neutron Physics and Nuclear Data for Reactors and Other Applied Purposes* (Harwell, United Kingdom, 1978), p. 438.
- [45] M. V. Bokhovko, L. E. Kazakov, V. N. Kononov, E. D. Poletaev, V. M. Timokhov, and A. A. Voevodskiy, *Vopr. At. Nauki Tekh., Ser.: Yad. Konstany* **1985**, 12 (1985).
- [46] T. Veerapaspong, M. Igashira, S. Mizuno, J.-I. Hori, and T. Ohsaki, *J. Nucl. Sci. Technol.* **36**, 855 (1999).
- [47] R. W. Hockenbury, W. R. Koste, and R. A. Shaw, *Bull. Am. Phys. Soc.* **20**, 560 (1975).
- [48] Yu. N. Trofimov, *Vopr. At. Nauki Tekh., Ser.: Yad. Konstany* **1993**, 17 (1993).
- [49] A. E. Johnsrud, M. G. Silbert, and H. H. Barschall, *Phys. Rev.* **116**, 927 (1959).
- [50] M. Afzal Ansari, R. K. Y. Singh, R. P. Gautam, and S. Kailas, *Ann. Nucl. Energy* **26**, 553 (1999).
- [51] C. Massimi *et al.*, *Eur. Phys. J. A* **50**, 124 (2014).
- [52] M. B. Chadwick *et al.*, *Nucl. Data Sheets* **112**, 2887 (2011).
- [53] Evaluated Nuclear Data Files, 2011, <http://www-nds.iaea.org/exfor.htm>
- [54] K. Shibata *et al.*, *J. Nucl. Sci. Technol.* **48**, 1 (2011).
- [55] Z. Bao, H. Beer, F. Käppeler, F. Voss, K. Wisshak, and T. Rauscher, *At. Data Nucl. Data Tables* **76**, 70 (2000).
- [56] I. Dillmann, M. Heil, F. Käppeler, R. Plag, T. Rauscher, and F.-K. Thielemann, *AIP Conf. Proc.* **819**, 123 (2006).
- [57] P. W. Merrill, *Astrophys. J.* **116**, 21 (1952).
- [58] M. Busso, R. Gallino, and G. J. Wasserburg, *Annu. Rev. Astron. Astrophys.* **37**, 239 (1999).
- [59] F. Herwig, T. Blöcker, D. Schönberner, and M. El Eid, *Astron. Astrophys.* **324**, L81 (1997).
- [60] N. Langer, A. Heger, S. Wellstein, and F. Herwig, *Astron. Astrophys.* **346**, L37 (1999).
- [61] S. Goriely and N. Mowlavi, *Astron. Astrophys.* **362**, 599 (2000).
- [62] S. Goriely and L. Siess, *Astron. Astrophys.* **421**, L25 (2004).
- [63] S. Goriely and L. Siess, in *Proceedings of IAU Symposium No. 228*, edited by V. Hill, P. François, and F. Primas (Cambridge University Press, Cambridge, England, 2005), p. 451.
- [64] F. Käppeler, K. A. Toukan, M. Schumann, and A. Mengoni, *Phys. Rev. C* **53**, 1397 (1996).
- [65] L. Siess and M. Arnould, *Astron. Astrophys.* **489**, 395 (2008).